INTERNATIONAL ATOMIC ENERGY AGENCY
UNITED NATIONS EDUCATIONAL, SCIENTIFIC AND CULTURAL ORGANIZATION

INTERNATIONAL CENTRE FOR THEORETICAL PHYSICS
34100 TRIESTE (ITALY) - P.O.B. 586 - MIRAMARE - STRADA COSTIERA 11 - TELEPHONES: 224281/2/3/4/5/6
CABLE: CENTRATOM - TELEX 460392-1

SMR/98 - 29

AUTUMN COURSE ON GEOMAGNETISM, THE IONOSPHERE AND MAGNETOSPHERE

(21 September - 12 November 1982)

IONOSPHERIC STRUCTURE

(Lecture 2)

Kenneth Davies

Space Environment Laboratory
National Oceanic and Atmospheric Administration
325 Broadway
Boulder, Colorado
U.S.A.

International Centre for Theoretical Physics

Autumn Course on Geomagnetism, the Ionosphere and Magnetosphere

Workshop on Radio Propagation in the Tropics

Lecture II

Ionospheric Structure

by

Kenneth Davies

2.1 Introduction

The electron density distribution in the ionosphere varies with height, with geographical location and with time. The structure of the ionosphere has been studied mostly by means of a sweep frequency radio sounder called an ionosonde that produces a record of virtual reflection height versus radio frequency. There are roughly 150 ionosonde stations as shown in Figure 2.1. Another powerful technique is the incoherent scatter radar (Farley 1970) that depends on small amounts of power scattered by individual electrons rather than by the bulk plasma. These radars are expensive to install and operate and there are (have been) only about six in operation. The longest incoherent scatter radar in operation is that at Jicamarca, Peru near the magnetic equator. Broadly speaking the ionosphere is divided geographically into the following zones: low latitudes, middle latitudes, auroral zones and polar caps -- see Figure 2.2 (Davies 1981). In height the ionosphere is generally divided into the D, E and F regions with the F layer being subdivided into F1 and F2 (see Figure 2.3). Other layers which may be present include: the cosmic ray or C-layer, sporadic or nocturnal E (E_S) G-layer above the F2 layer. The temporal behavior is divided into diurnal (sunlit, dark) seasonal (winter, summer and equinox), and the sunspot (11-year) variation. We shall discuss these features in this and succeeding lectures.

2.2 Ionospheric Sounding

The ionosonde is a radio transmitter and receiver which sweeps in frequency from below 1 MHz to about 30 MHz and measures the time of flight, t, of an emitted radio echo to and from the ionosphere. The virtual, or group, height of reflection h' is defined by

$$h' = \frac{1}{2} c t \qquad 2.1$$

as if the pulse travelled with the free space speed c. The photographic output of an ionosonde, called an ionogram, is illustrated in Figure 2.4 (Davies 1965). The most prominant characteristics are: (a) the existence of several layers (b) the penetration or critical frequencies (c) the presence of magneto-ionic traces and (d) the virtual heights of the different layers. The ordinary, extraordinary and z-wave critical frequencies are related by (equations 1.23 and 1.24).

$$f_o^2 = f_x^2 - f_x H_H \qquad 2.2$$

$$f_z = f_x - f_H \qquad 2.3$$

When f_o, $f_x \gg f_H$

$$f_x \approx f_o + \frac{1}{2} f_H \qquad 2.4$$

The z-trace is rarely seen in low latitudes. Because the strength of the earth's magnetic field decays with altitude the separation of the critical frequencies may differ slightly for different layers. By suitable inversion techniques the electron density profile can be obtained from an ionogram. The real height is always less than, and may be very much less than, the virtual height. The latter can be measured by the frequency dependence of phase ϕ (equation (1.12)

$$h' = \frac{1}{2} c \frac{d\phi}{df} \qquad 2.5$$

Sample ionograms for low- and high-latitudes are shown in Figure 2.5.

In recent years ionosondes have been improved by employing modern digital techniques to control: frequency synthesis, pulse shape, frequency sweep, phase measurement, amplitude measurement etc. Digital ionograms are recorded and stored on magnetic tape (Grubb 1979, Bibl and Reinisch 1978, Dudeney 1981) and a sample is shown in Figure 2.6. From the amplitude measurements, together with suitable calibration one can determine the variation of absorption with frequency. From the phase measurements it is possible to separate the ordinary and extraordinary waves and to determine the angle of arrival using appropriately arranged antennas -- see Figure 2.7. The doppler shift, Δf, caused by time changes in the reflection area is given by

$$\Delta f = -\frac{d\phi}{dt} \qquad 2.6$$

where ϕ is in cycles

2.3 Layer Structure

2.3.1 The D layer

The D layer is important in the propagation of radio waves: (1) because it absorbs energy from radio waves and (2) because it reflects long and very-long waves. The D layer lies between about 50 km and 90 km. This definition is, of course, arbitrary and it is important to realize that no sharp boundary exists between one layer and another. The normal ionosonde technique cannot be used to determine electron density profiles in the D region because the density there requires such low frequencies for probing that they would be completely absorbed. Techniques which can be used to obtain N(h) profiles include cross-modulation (Lee and Ferraro 1969), partial reflection (Belrose 1970) and incoherent scatter (Farley 1970). Some examples of daytime profiles are given in Figure 2.8. George (1971) showed that the D region is geomagnetically controlled, there are HF absorption maxima near 20° north and 20° south of the magnetic equator.

2.4 The E layer

The E layer is very important in the reflection of medium-and high-frequency waves. It may also act to prevent waves from reaching the F2 layer and, thus, produce a lower cut-off frequency for HF radio circuits. Sporadic-E propagation is occasionally observed as high as 150 MHz and TV signals can be transmitted over 1500 km.

During the day the variation of the critical frequency is given by

$$f_0 E = 0.9\,[(180 + 1.44R)\cos\chi]^m \text{ MHz} \qquad 2.7$$

Here R is the Zurich sunspot number (12 month running mean), χ is the solar zenith angle and the exponent m varies from about 0.20 to about 0.30.

Some sample daytime N(h) profiles for the E region are shown in Figure 2.9. It is not possible to obtain direct ionogram information about the lower E-region (85-100 km) because waves reflected there are heavily absorbed. By day the height of maximum electron density lies between 100 km and 120 km but this is often difficult to pin down because of the presence of strong sporadic-E echoes. Evidence indicates that there is a "valley" in the N(h) distribution above the E-layer peak.

After sunset the critical frequency of the E layer decreases rapidly but reaches a minimum value of about 0.5 MHz several hours before sunrise. At Boulder there appears to be little or no seasonal variation of this nighttime minimum but there is a sunspot dependence. On the average f_0E is about 0.25 MHz lower at sunspot minimum with an average predawn minimum of 0.5 MHz.

Unlike the E layer critical frequency the sporadic-E critical frequency is highly variable with respect to location and time. The critical frequency f_0E_s can vary from less than f_0E ($\approx$ 2-3 MHz) to > 30 MHz at a given location. Monthly median maps of f_0E_s have been constructed for various UT by Leftin, Ostrow and Preston (1968). Because of the high variability these authors give

also maps of the lower and upper deciles of the monthly distributions. World patterns of occurrence of E_s indicate that the variations of the different types of E_s are influenced by the geographical location -- Figure 2.10. Some types of E_s, such as that which occurs near the magnetic equator, are well behaved and are a regular feature of the ionosphere. One problem with sporadic E is that it is often partially transparent and the upper layers can be seen through it on frequencies above a "blanketing" frequency f_bE_s. Maps of f_oE_s (medians and deciles) have been constructed by Leftin and Ostrow (1969).

2.5 The F1 Layer

The F1 layer is observed only during the day; it is more pronounced in summer than in winter, at high sunspot numbers and during ionospheric storms when foF2 is low. The F1 critical frequency is well behaved. To a first approximation

$$foF1 = (4.3 + 0.01\ R)\ \cos^{0.2} \chi \qquad 2.8$$

$$\text{or} \quad foF1 = C \cos^{n} \chi \qquad 2.9$$

in which C and n depend on R and on geomagnetic latitude. A more sophisticated model has been given by Rosich and Jones (1973).

2.6 The F2 Layer

Of all the ionospheric layers the F2 layer is by far the more important both because of the higher frequencies reflected from it and because of its height which gives rise to longer hops. The critical frequencies of the F2 layer are quite variable and do not depend in any simple fashion on the solar zenith angle. They are characterized by marked geomagnetic control in low latitudes, as in Figure 2.11, and by a winter "anomaly" in middle latitudes in which winter daytime values are higher than in summer -- Figure 2.12.

The f_xF2, or zero distance maximum frequency, and other characteristics of the F2 layer have been expressed in terms of polynomial functions of latitude,

longitude and universal time (CCIR 1978) and are stored in the form of computer software (Haydon et al 1976), see Figure 2.13. Note the marked geomagnetic control (humps) on either side of the magnetic equator. This is brought about by the electromagnetic vertical drift resulting from a west-to-east electric field brought about by electric polarization in the E layer. The plasma is lifted up over the equator and then "slides" down the magnetic field to produce the peaks around ± 15° of magnetic latitude. In terms of electron density distribution this produces a dome over the equator giving unusual radio ray paths -- see Figure 2.14. Sample electron density profiles above Jicamarca, Peru for day are shown in Figure 2.15 and night in Figure 2.16.

In high latitudes, the F2 layer -- and other layers -- is dominated by the influence of the magnetosphere a region of energetic electrons and protons surrounding the earth. Magnetospheric electric fields, dawn-to-dusk, produces a day to night $\underline{E} \times \underline{B}$ convection over the polar caps which is particularly important in maintaining the F2 layer during the long winter night. Charged particles also produce ionization in the night auroral ionosphere. The ionosphere, in high latitudes, exhibits certain features such as: the nighttime trough or slot of low electron densities; the auroral zone characterized by spread F; the magnetospheric cleft where solar particles have more-or-less direct access to the ionosphere. Ionograms frequently exhibit spread-F which indicates the presence of relatively small scale plasma irregularities that scatter the incident radio signals.

During evenings, near the geomagnetic equator, marked spread F is observed on ionograms indicating the presence of intense (depletions?) plasma irregularities -- Figure 2.17. This is preceded by or accompanied by the presence of plumes on the Jicamarca incoherent scatter radar records -- Figure 2.18.

References

Belrose, J. S., 1970, Radio wave probing of the ionosphere by the partial reflection of radio waves, J. Atmos. Terr. Phys., 32, (4), 567-596.

Bibl, K. and B. W. Reinisch, 1978, The universal digital ionosonde, Radio Sci., 13, (3), 519-530.

CCIR, 1979, CCIR atlas of ionospheric characteristics, Rep 340-3, Int. Telecommun. Union, Geneva.

Davies, K., 1965, Ionospheric Radio Propagation, NBS Monograph 80, U. S. Gov't Printing Office, Washington, D. C.

Davies, K., 1981, Review of recent progress in ionospheric predictions, Radio Sci., 16, 1407-1430.

Dudeney, J., 1981, The ionosphere -- a view from the pole, New Scientist, 714-717.

Farley, D. T., 1970, Incoherent scattering at radio frequencies, J. Atmos. Terr. Phys., 32, (4), 693-704.

George, P. L., 1971, The global morphology of the quantity $\int N v dh$ in the D and E-regions of the ionosphere, J. Atmos. Terr. Phys., 33, 1893-

Grubb, R. N., 1979, The NOAA SEL HF Radar System (Ionospheric Sounder), NOAA Tech Memo ERL/SEL-55.

Haydon, G. W., M. Leftin and R. Rosich, 1976, Predicting the performance of high frequency sky wave telecommunications systems, OT Report 76-102, U. S. Dep't of Commerce.

Lee, H. S. and A. J. Ferraro, 1969, Winter D-region electron concentration and collision frequency features obtained with high power interaction measurements, J. Geophys. Res., 74, 1184-1194.

Leftin, M., S. M. Ostrow and C. Preston. (1968) Numerical maps of f_0E_s for solar cycle minimum and maximum, ESSA Tech. Rep. ERL-73-ITS-63.

Leftin, M. and S. M. Ostrow, 1969, Numerical maps of f_bE_s for solar cycle minimum, ESSA Tech. Rep. ERL-124-ITS-87.

Rosich, R. K. and W. B. Jones, 1973, The numerical representation of the critical frequency of the F1 region of the ionosphere, OT Report 73-22, U. S. Dep't of Commerce/Office of Telecommunications, Washington, D. C.

Woodman, R. F. and C. LaHoz, 1976, Radar observations of F-region equatorial irregularities, J. Geophys. Res., 80, 4383-4386.

Figure Captions

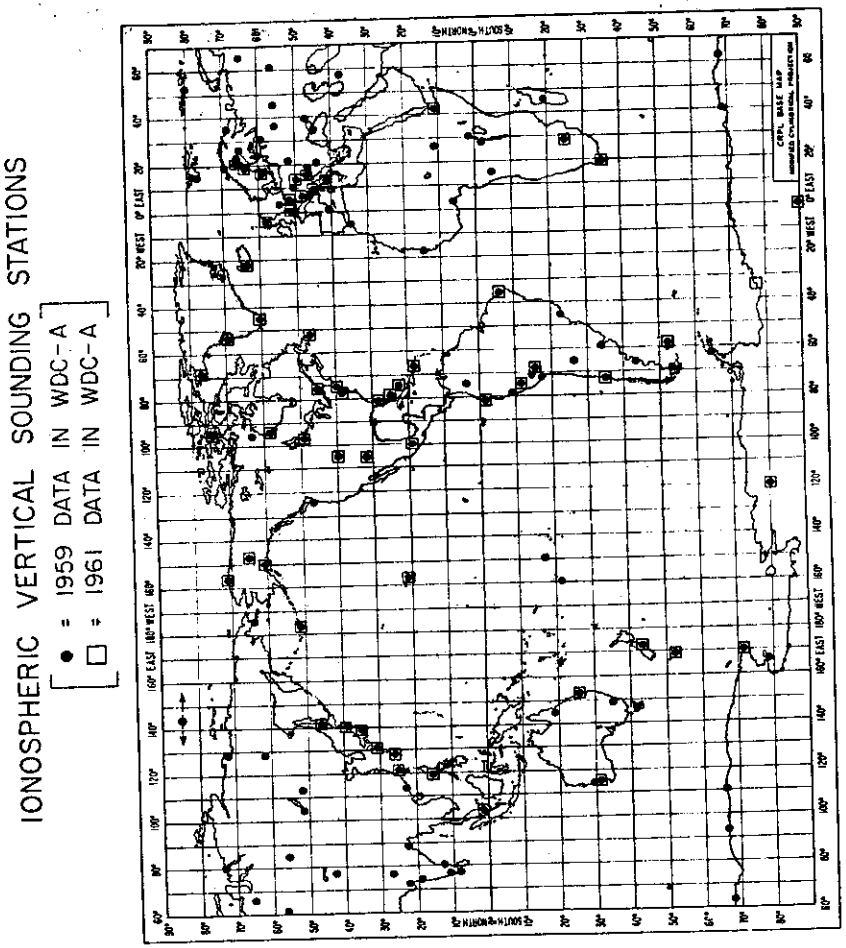

Fig. 2.1 Ionospheric vertical sounding stations

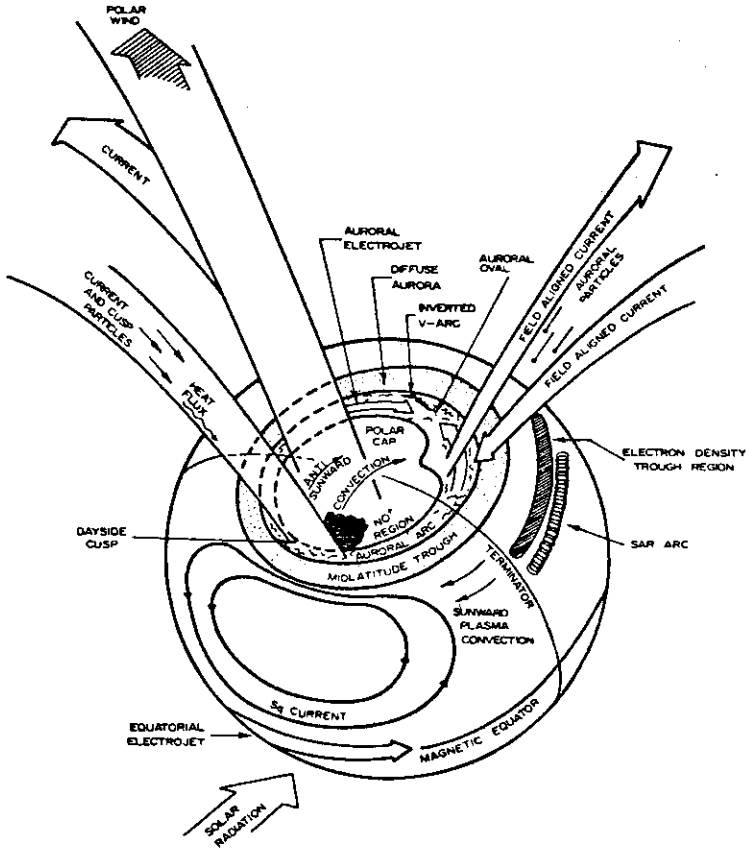

Figure 2.2 A schematic view of high latitude processes of special interest to ionospheric scientists and communicators

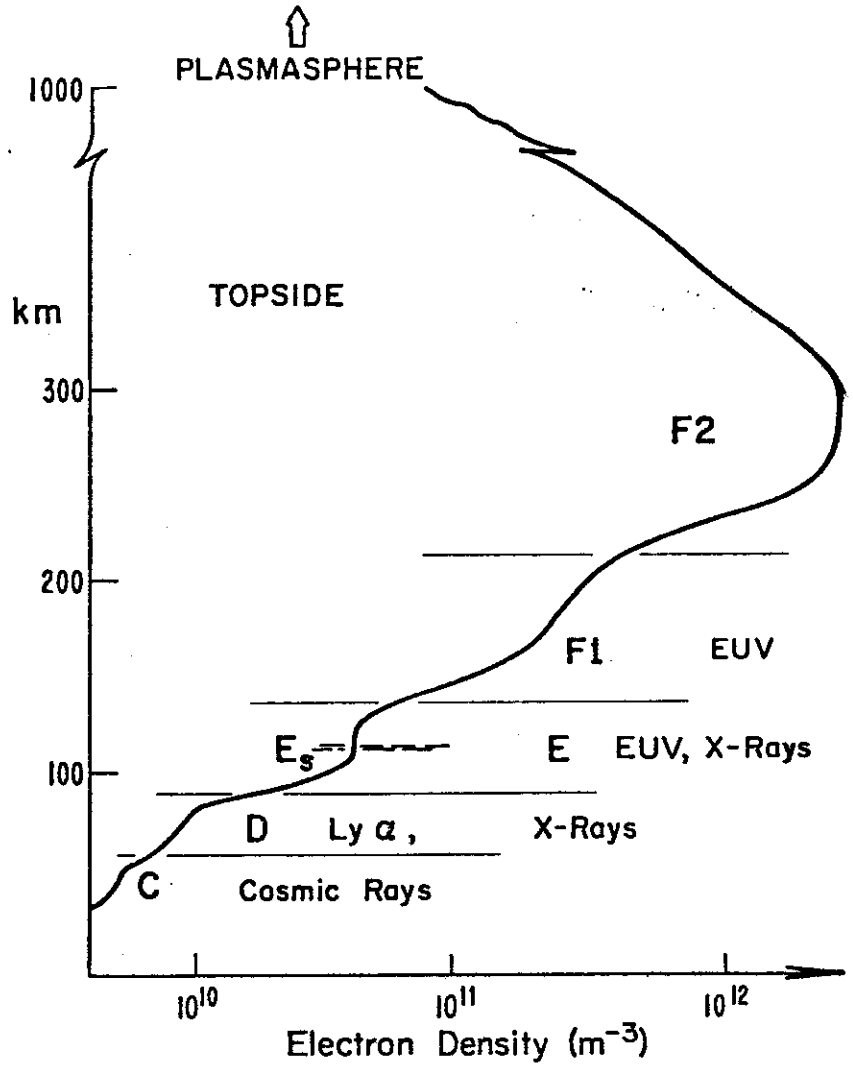

Figure 2.3 Structure of the ionosphere

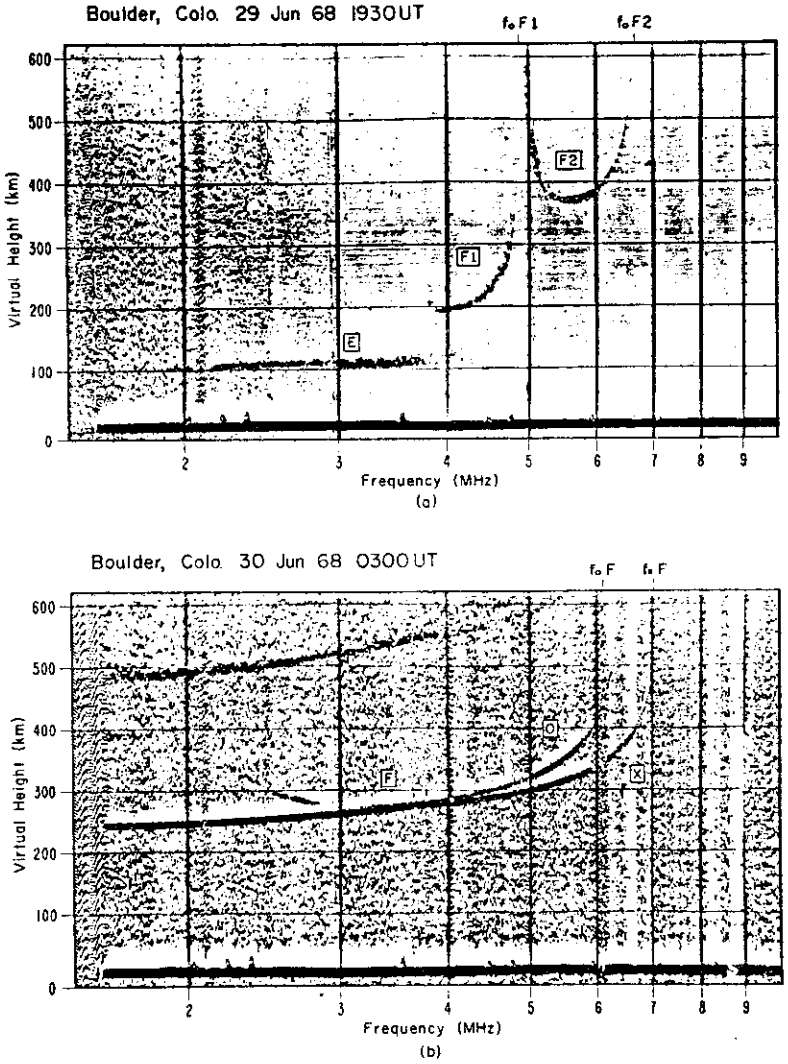

Figure 2.4 Sample ionograms showing layers and magnetoionic traces

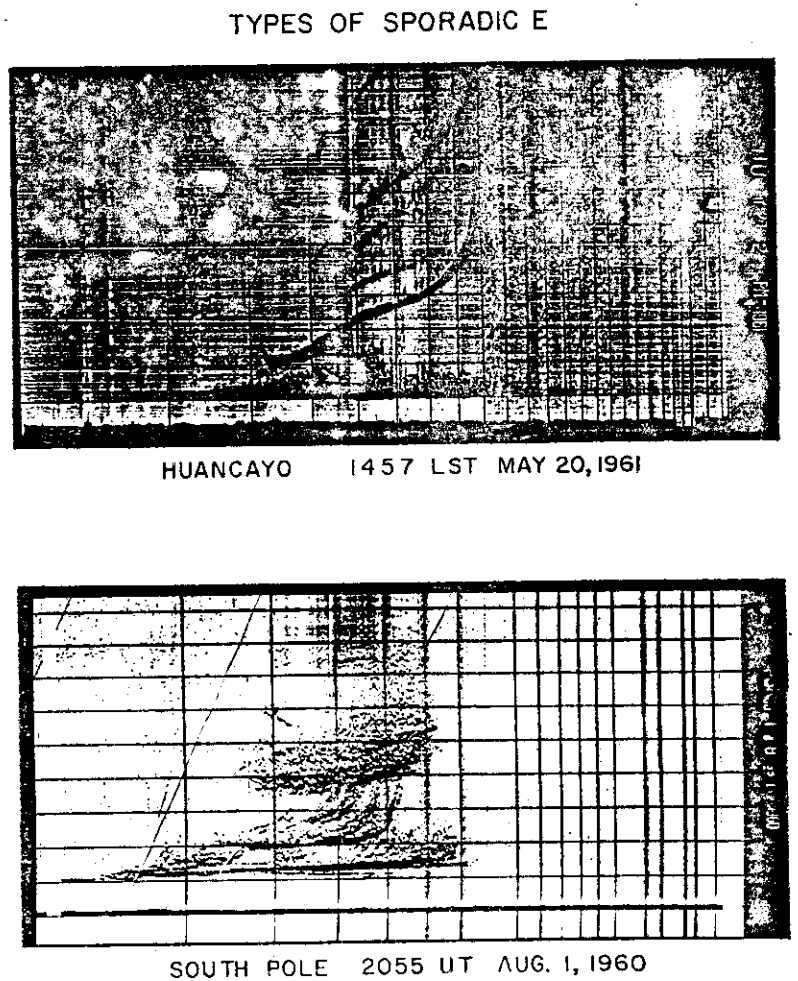

Fig. 2.5 Types of sporadic E

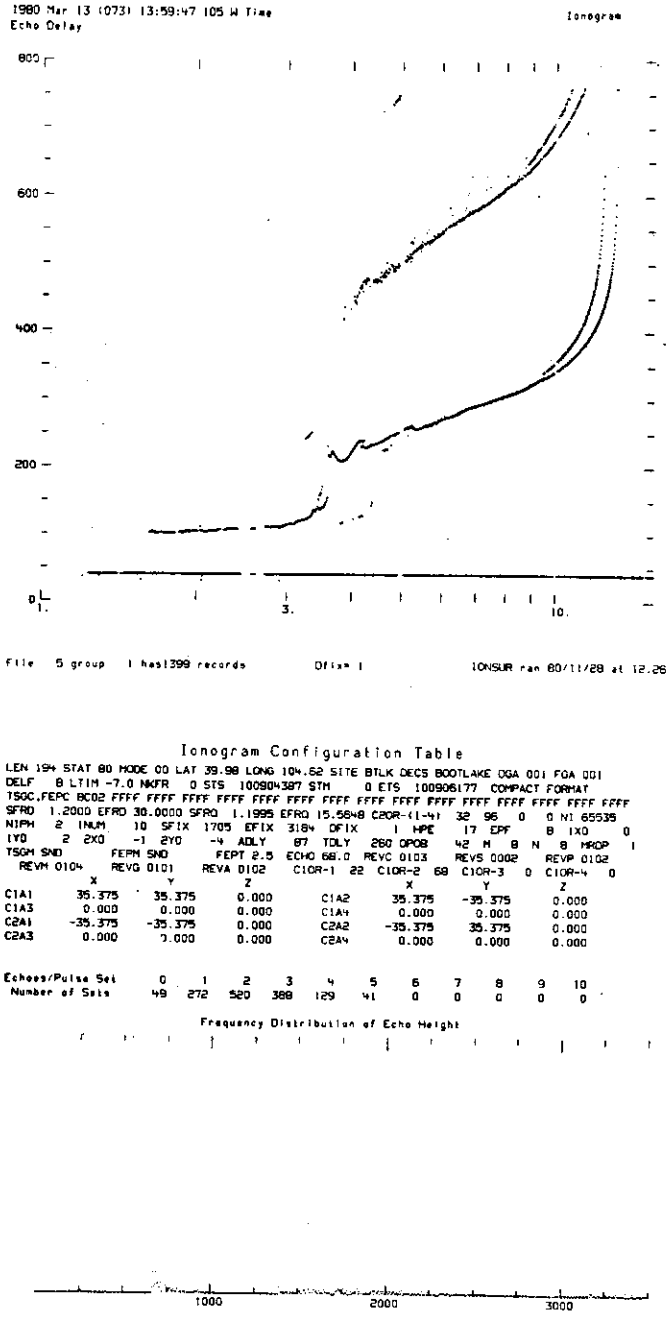

Fig. 2.6 Digital ionogram

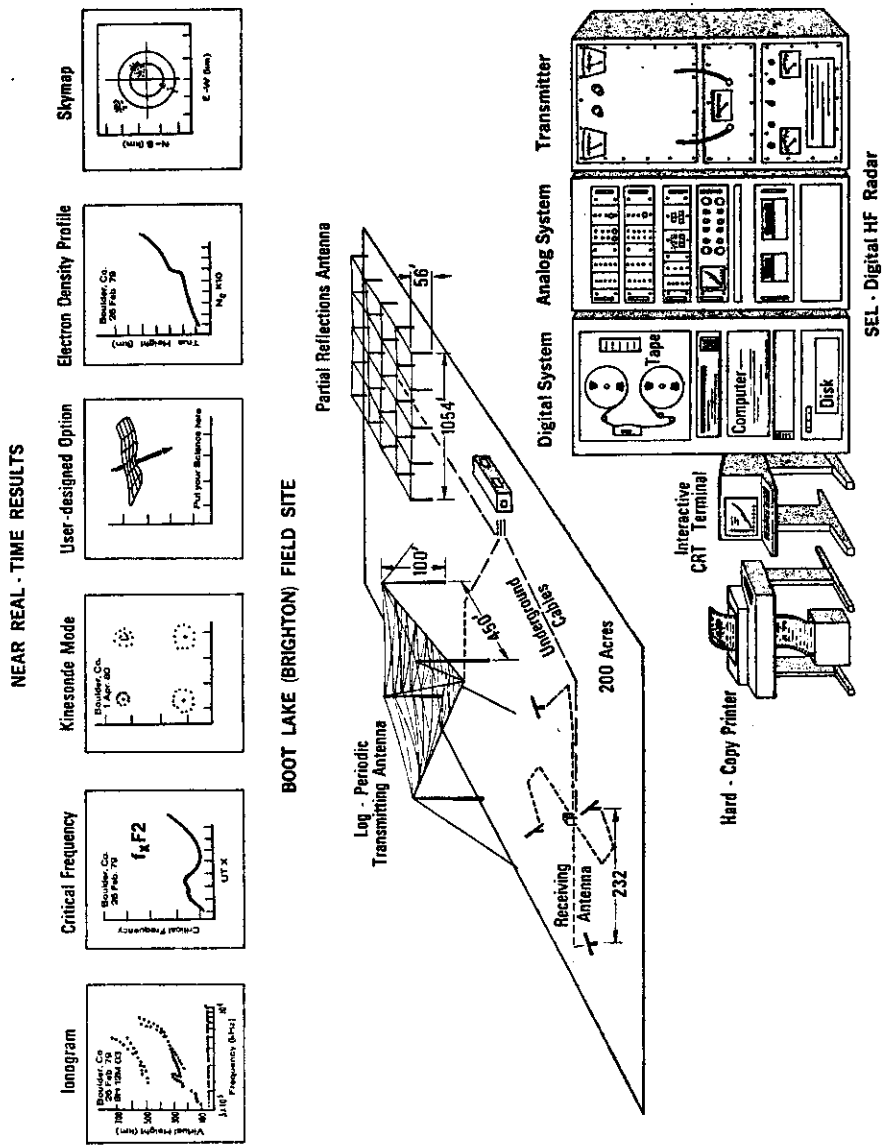

Fig. 2.7 SEL Digital HF Radar

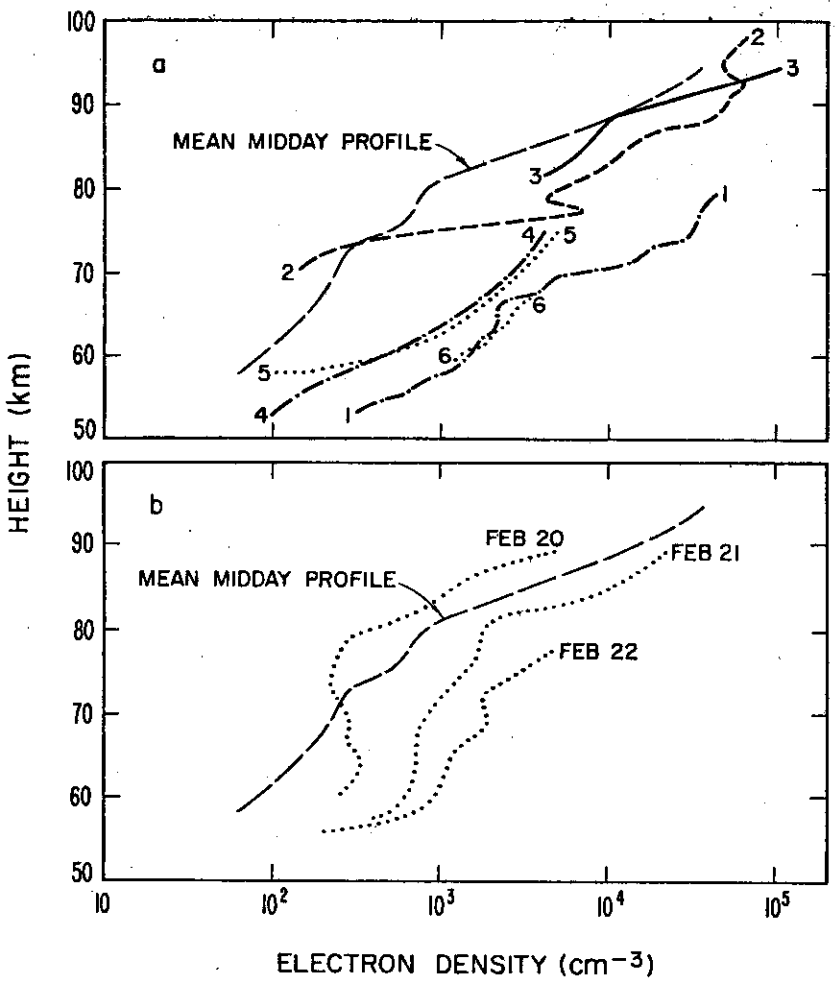

Fig. 2.8 Sample daytime electron density profiles in the D region

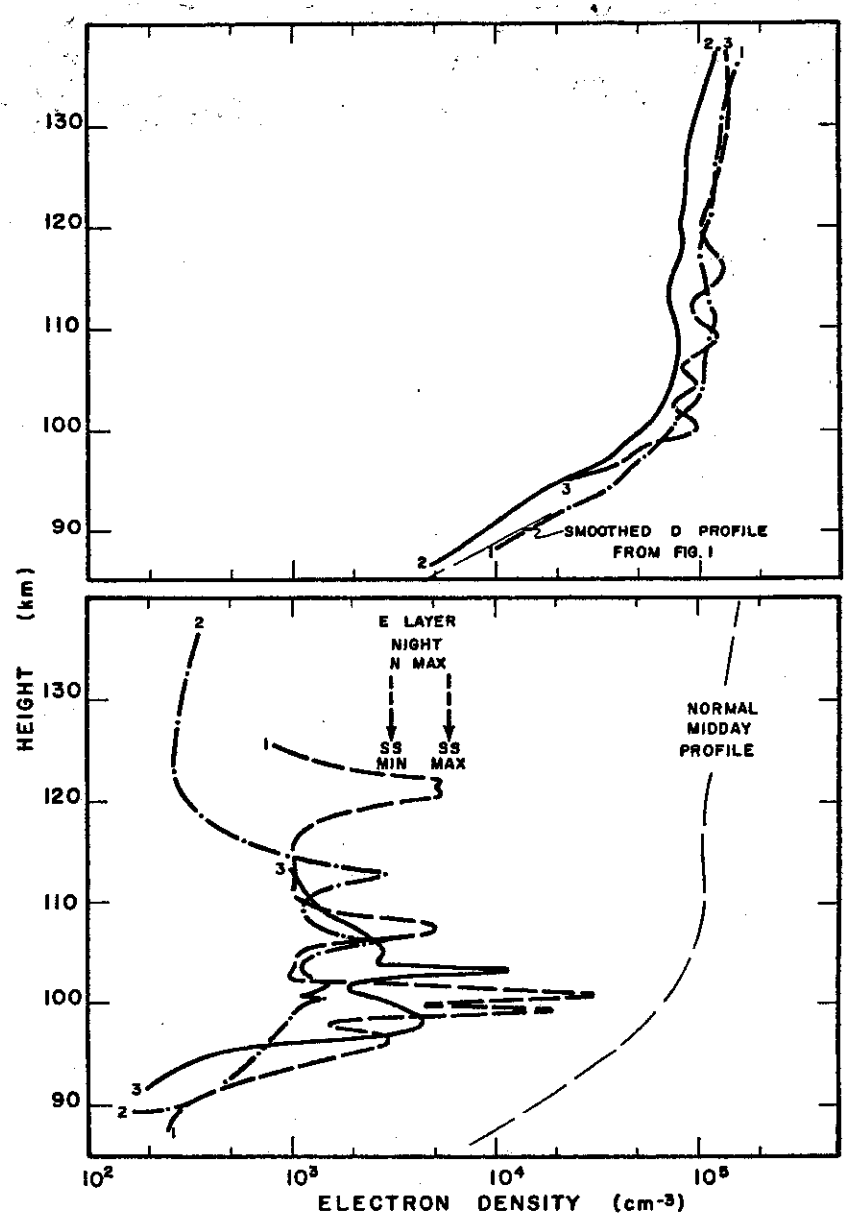

Fig. 2.9 Sample day and night N (h) profiles for the E region

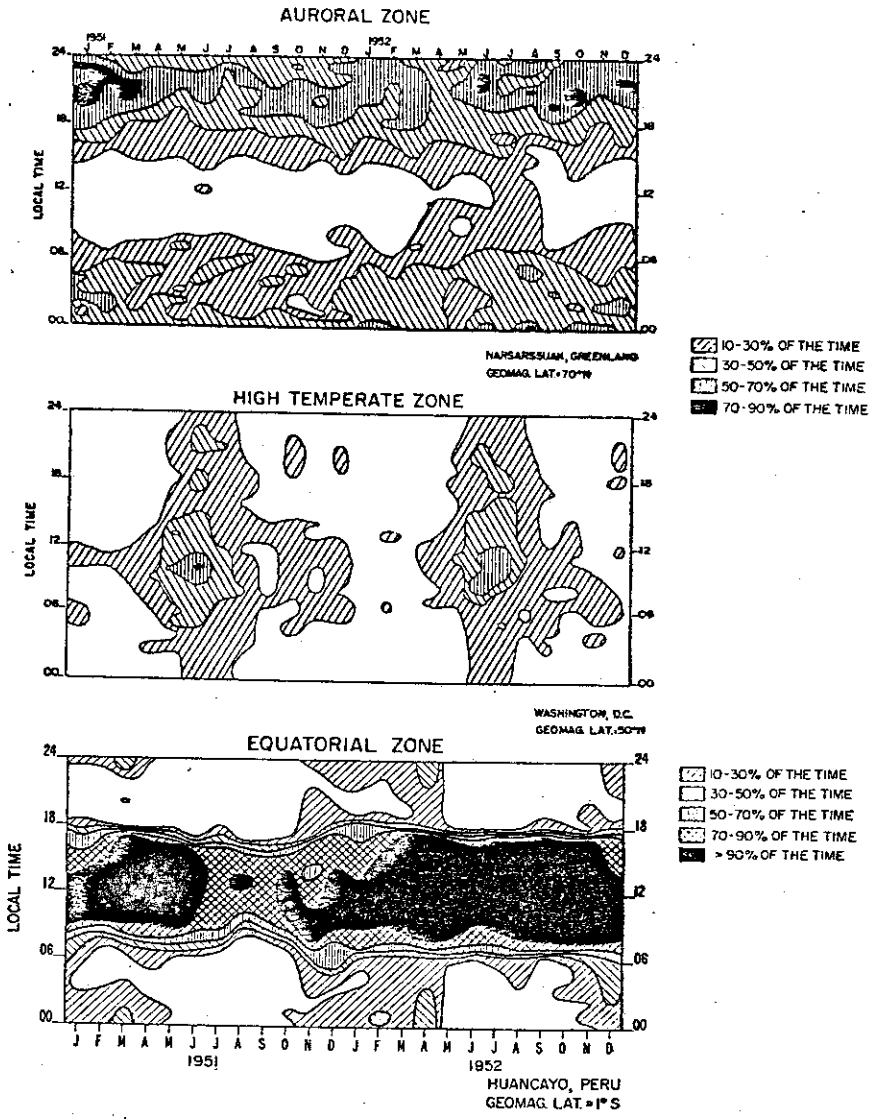

Fig. 2.10 Occurrence of sporadic E in different geographic zones

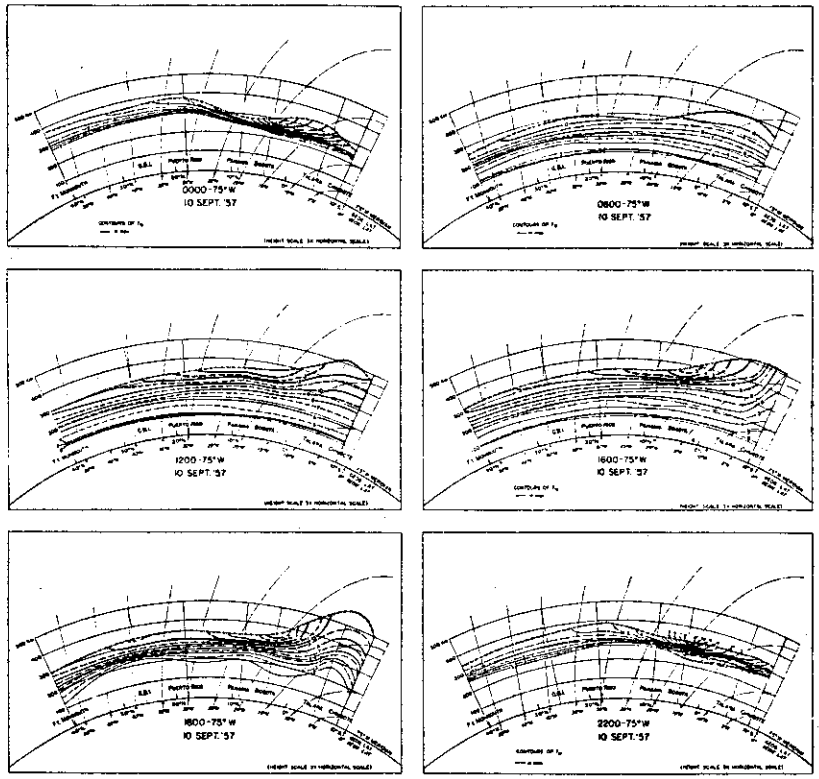

IONOSPHERIC SECTIONS ALONG 75th GEOGRAPHIC MERIDIAN, 40°N-10°S

Fig. 2.11 Ionospheric sections along 75th geographic meridian 40°N-10°S

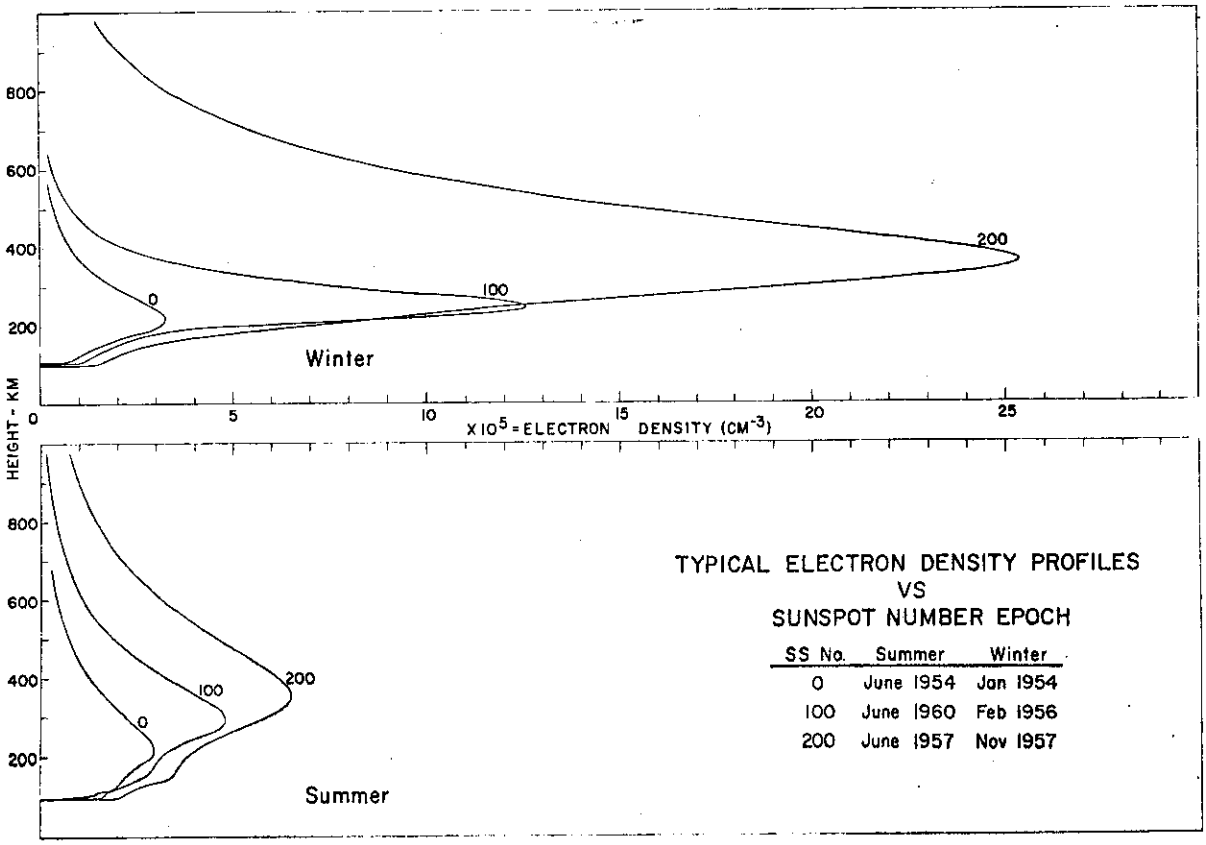

Fig. 2 12 Typical electron density profiles vs. sunspot number epoch

(21)

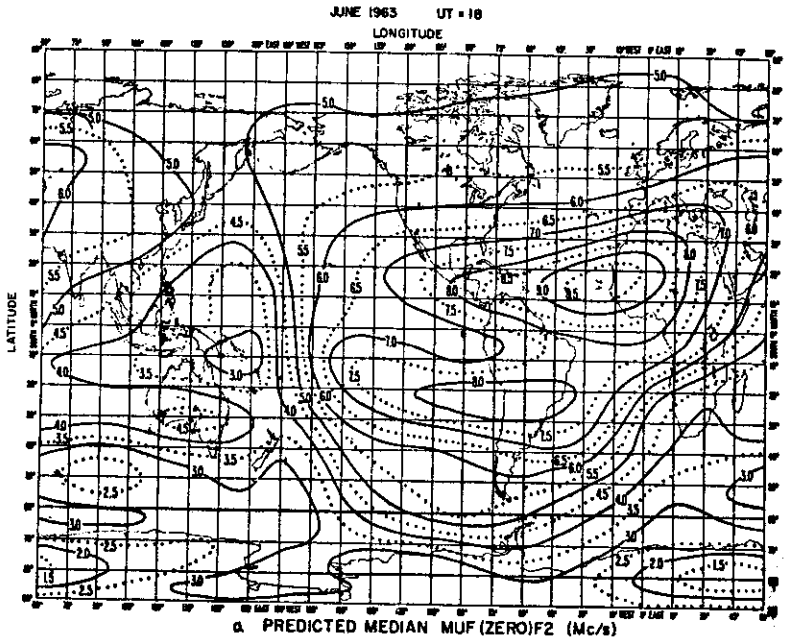

Fig. 2.13 Numerical map of the distribution of MUF(zero)F2, or fxF2, in megahertz

(22)

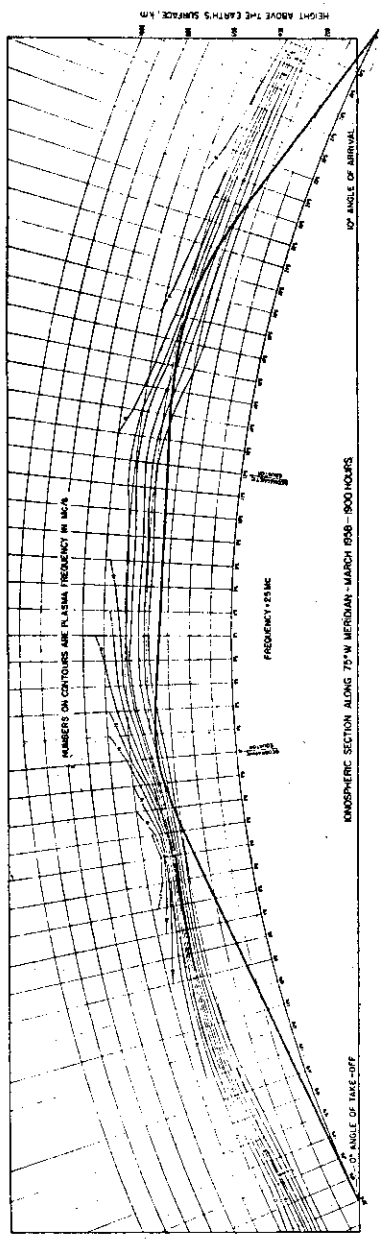

Fig. 2.14 Sample ray path across the equatorial anomaly

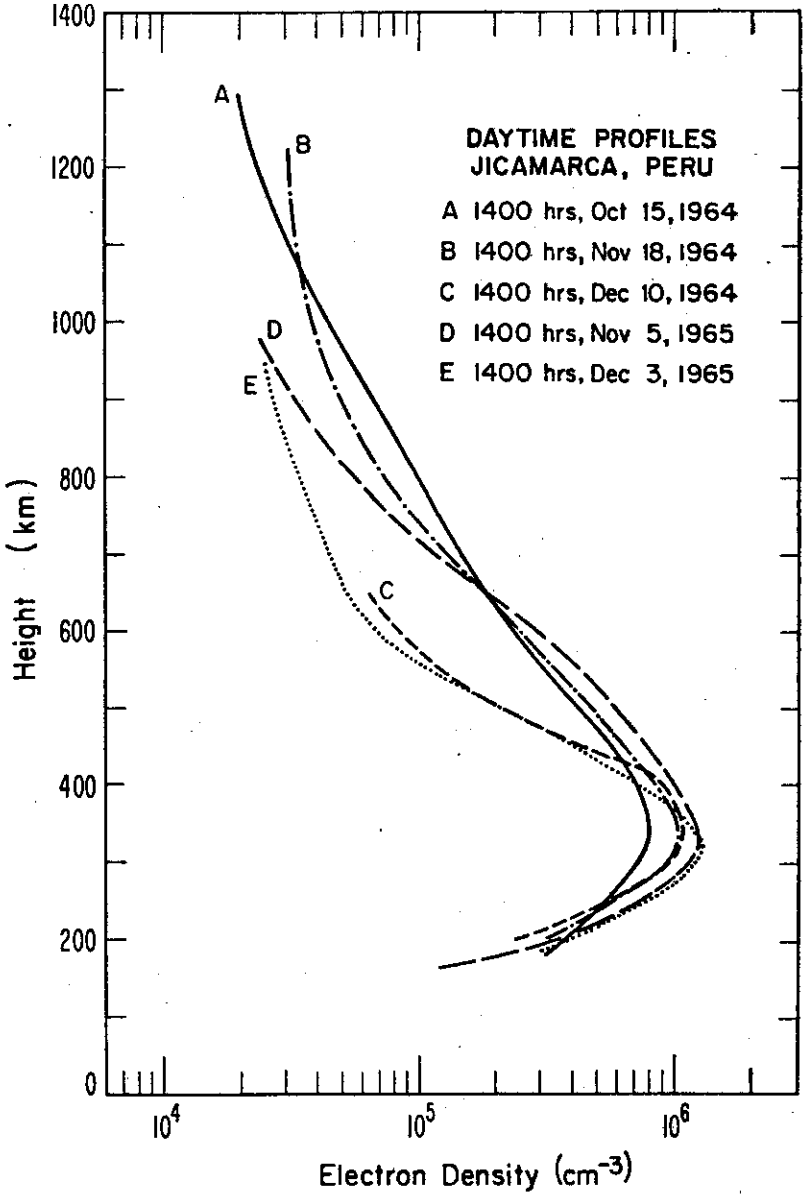

Fig. 2.15 Sample daytime electron density profiles over Jicamarca, Peru obtained by incoherent scatter radar

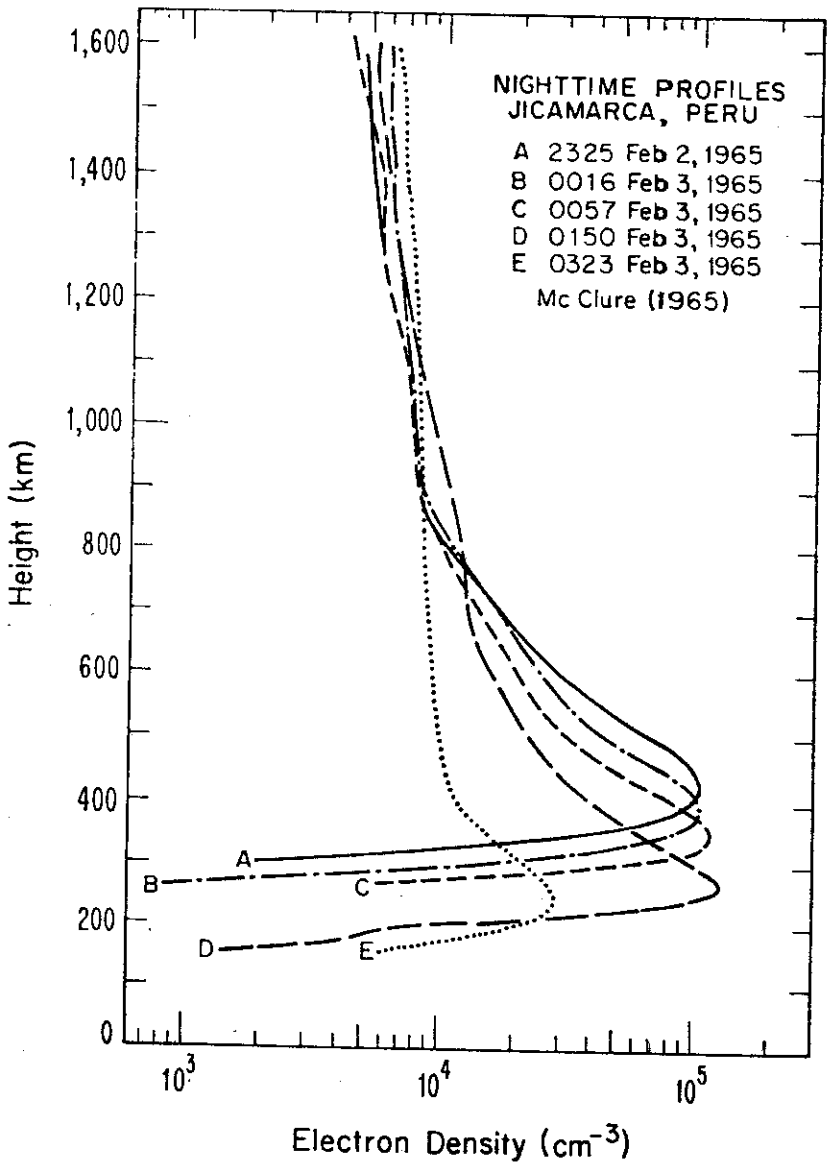

Fig. 2.16 Sample nighttime electron density profiles over Jicamarca, Peru obtained by incoherent scatter radar

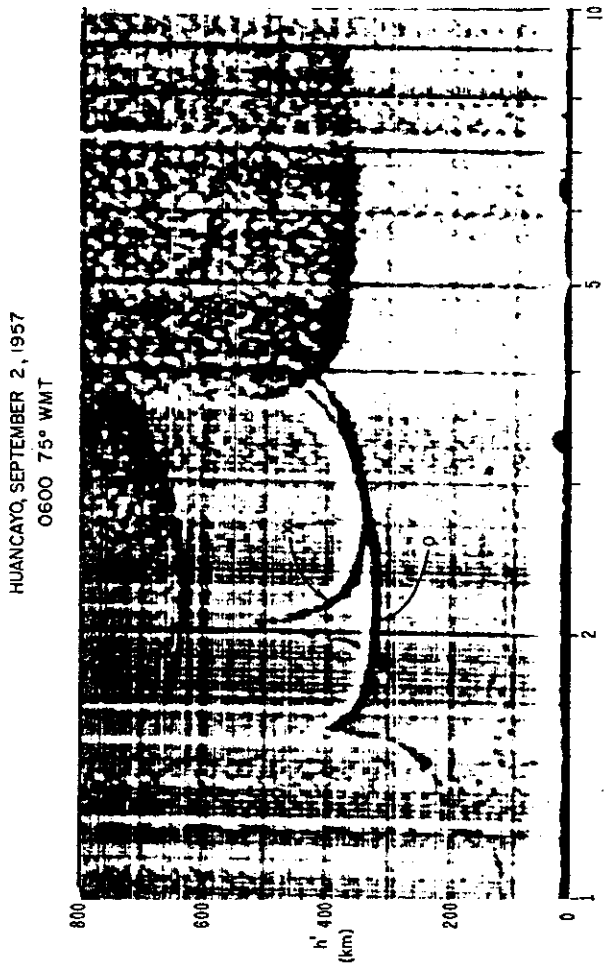

Fig. 2.17 Ionogram showing equatorial spread F

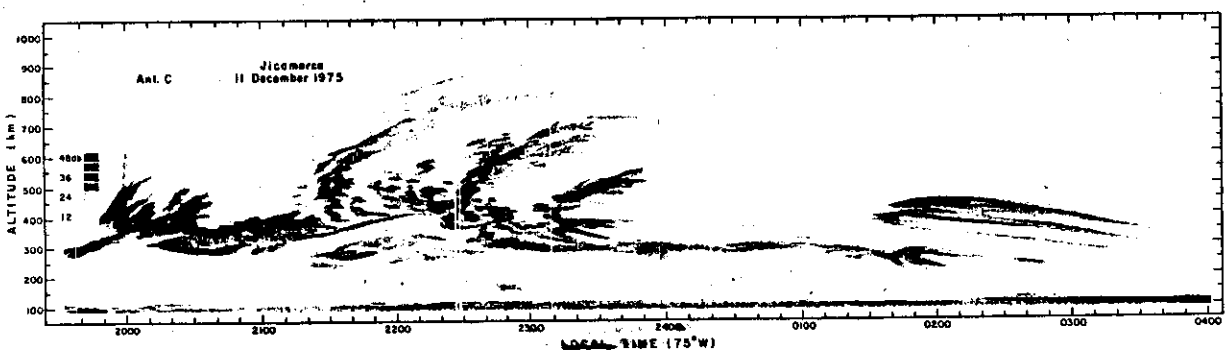

Fig. 2.18 Plumes observed by the Jicamarca incoherent scatter radar at time of spread F and transionospheric radio scintillation